Regular Article

IMMUNOBIOLOGY

CD138 mediates selection of mature plasma cells by regulating their survival

Mark J. McCarron,[1] Pyong Woo Park,[2,3] and David R. Fooksman[1]

[1]Department of Pathology, Albert Einstein College of Medicine, Bronx, NY; and [2]Division of Newborn Medicine and [3]Division of Respiratory Diseases, Children's Hospital, Harvard Medical School, Boston, MA

Key Points

- CD138 is required for survival of ASCs and long-term humoral immunity.

Antibody secreting cells (ASCs) are critical effector cells and long-lived sentinels for immune memory. ASCs are highly dependent on exogenous soluble factors such as interleukin-6 (IL-6) and APRIL, to prevent their cell death. We have found that the canonical surface marker of ASCs, CD138 (syndecan-1), which is upregulated during ASC maturation, is required in a cell-intrinsic manner to mount an effective long-term humoral immune response following immunization. Surface expression of CD138 increased heparan sulfate levels on ASCs, which are known to bind pro-survival cytokines, leading to increased survival in a cell-intrinsic manner in vivo. In IL-6 and APRIL-deficient hosts, ASCs underwent extensive apoptosis independently of CD138 expression. We propose a model in which CD138 expression on fully mature ASCs provides a selective survival advantage over less mature, newly minted ASCs, by enhancing pro-survival cytokine signaling. (*Blood*. 2017;129(20):2749-2759)

Introduction

Antibody secreting cells (ASCs) are terminally differentiated B cells that produce high quantities of antibody, critical for pathogen clearance and long-lasting prophylaxis against secondary challenge.[1] ASCs, comprising both mature plasma cells (PCs) and less mature plasmablasts, can easily be identified as mononuclear cells with highest surface expression of CD138, also known as syndecan-1 (sdc1), which is upregulated over a 1000-fold during ASC differentiation.[2] However, CD138 is also expressed at high levels in epithelial cells and at lower levels on a variety of cell types, including endothelial cells and fibroblasts, with a diverse array of functions.[3,4] Thus, although the function of CD138 has been studied in the context of many diseases,[4] understanding the cell-intrinsic function of CD138 on ASCs has proven problematic.

CD138 is a member of the syndecan family of type I transmembrane proteoglycans, comprised of a core protein, and glycosylated with chondroitin and heparan sulfate (HS) moieties.[5] Among its many functions, CD138 has been implicated in wound healing,[6] cell adhesion,[7] endocytosis,[8] and may translocate to the nucleus.[9] Hundreds of proteins can bind to CD138, including extracellular matrix components, integrins,[10] growth factors,[11] cytokines,[12] and chemokines.[13] The ectodomain of CD138 can also be shed, which can affect its function and stability.[3,14]

Interest in CD138 function has focused greatly on its role in cancers, particularly in vitro models of multiple myeloma and breast cancer. In myeloma, CD138 has been shown to bind the survival factor APRIL,[15] and act as a co-receptor to bind growth factors, such as hepatocyte growth factor and epidermal growth factor to promote cell survival and proliferation in the bone marrow (BM).[16,17] Increased serum levels of shed, soluble CD138 is linked with poorer overall survival in myeloma.[18]

Despite a plethora of studies on CD138 in other contexts, and its high expression on ASCs, its function on normal ASCs generated during humoral immune responses is unknown, particularly in vivo. Some have speculated that CD138 might not be required for normal PC function,[19] given the lack of an overt pathology in unchallenged sdc1-deficient mice maintained in pathogen-free conditions.[4] Nevertheless, using a cell transfer model, we find a direct cell-intrinsic role for CD138 on ASC survival in vivo, by promoting pro-survival cytokine signaling that contributes to the selection of more mature ASCs during immune responses.

Materials and methods

Mice

C57BL/6 CD45.1$^+$ (B6.SJL) mice were used as recipients (Charles River). IL-6$^{-/-}$ and APRIL$^{-/-}$ mice were obtained from The Jackson Laboratory. Sdc1$^{-/-}$,[20] B1-8^{high},[21] and Blimp1-YFP[22] mice were generated previously and bred in-house. For chimeric animals, 2 million donor BM cells were IV injected into lethally irradiated recipient mice and used 6 weeks later as recipients. The Institutional Animal Care and Use Committee approved the animal work conducted in this study.

Cell preparation and immunization

For cell transfer experiments, recipient mice were immunized intraperitoneally (IP) with ovalbumin (OVA) (50 μg) precipitated in Alum (Thermo Scientific) to generate OVA-specific T cells. After 2 to 4 weeks, mice received IV adoptive transfer of 2×10^6 naive B cells that were purified by CD43 depletion (Miltenyi Biotec). The following day, mice were boosted with 50 μg/mouse

---

of nitrophenyl (NP)-conjugated OVA (NP-OVA) (NP[16]; Biosearch Technologies) by subcutaneous injections distributed into the footpads, handpads, and base of the tail to target draining lymph nodes (LNs). IP injection of NP-OVA emulsified in alum for spleen immunization. For NP-specific antibody measurements, mice were injected subcutaneously into the footpads, handpads, and base of the tail with NP-OVA directly emulsified in alum. For examination of ASCs in BM on day 28, mice were immunized with NP-keyhole limpet hemocyanin (KLH) emulsified in alum. For in vitro assays, purified naïve B cells were cultured at 37°C in RPMI media with 10% fetal calf serum, penicillin-streptomycin-L-glutamine, β-mercaptoethanol (0.05 mM), and lipopolysaccharide (LPS) (20 μg/mL; Sigma). Human blood samples were obtained from de-identified healthy donors.

Antibodies and flow cytometry

Antibodies for human and mouse staining were obtained from eBioscience, BioLegend, or BD Biosciences, and were titrated for saturating concentrations and used with fragment constant blocking antibody. For human staining, CD138 (clone B-A38) from Bio-Rad Laboratories was used. For Ki67 and Foxp3 staining, Foxp3 Staining Kit was used (eBioscience). For caspase 3, B-cell lymphoma 2 (Bcl-2), and mantle cell leukemia 1 (Mcl-1) staining, a cytofix/cytoperm kit (BD) was used. Annexin V kit (eBioscience) was used as directed. For phosphorylated STAT 3 (pSTAT3) protein staining, cells were serum starved in RPMI (30 minutes), incubated with mouse IL-6 or IL-21 (10 ng/mL, 20 minutes; BioLegend), fixed in 2% paraformaldehyde, permeabilized with ice-cold methanol, washed, and antibody stained. For HS quantification, 10E4 antibody (Amsbio) was conjugated to Alexa 647 in-house and used to stain cells, with or without heparinase III (2U; Sigma) pretreatment. For cell division assay, B cells were labeled with CellTrace Violet. Fluorescent counting beads (Spherotech) were routinely used. Flow cytometric analysis was carried out using a BD LSR II or FACSCalibur (BD Biosciences).

Enzyme-linked immunosorbent assay (ELISA)

Immunoglobulin M (IgM)- and IgG-specific antibodies against NP were detected, and NP-bovine serum albumin (BSA) (either NP16 or NP3) was titrated and used as a capture antigen at 2 μg/mL. Serial dilutions of serum samples were plated at 1:1000 starting concentration. Purified NP-specific antibody, 9T13, was used to quantify antibody levels. IgG- or IgM-horseradish peroxidase (Jackson ImmunoResearch Laboratories) was used with tetramethylbenzidine substrate (Calbiochem) for detection.

Enzyme-linked immunospot (ELISPOT) assay

Plates (MAHAS4510; Millipore) were coated with NP(23)-KLH (20 μg/mL; Biosearch Technologies) and incubated overnight at 4°C. Plates were washed with phosphate-buffered saline and blocked overnight with phosphate-buffered saline and 1% BSA. Cells (diluted from 500 000 per well) were plated and incubated overnight at 37°C, and washed and detected with anti–IgG-horseradish peroxidase with tetramethylbenzidine (Mabtech, Inc.).

Two-photon microscopy

For imaging experiments, mice were prepared as previously described.[22] To analyze apoptosis in vivo, XYZT movies were manually analyzed for the acute appearance of cell blebbing and debris by a trained observer, who was blind to the conditions. Apoptotic events were normalized vs time and measurements pooled between several movies from 3 independent experiments per condition.

Statistical analysis

Mean value and standard error of the mean (SEM) were calculated. Unpaired, two-tailed Student t tests were used to calculate significance between the 2 groups.

Results

### Deficient antigen-specific antibody response in mice lacking CD138 expression

The surface expression of CD138 is a hallmark of ASC maturation[2]; however, there are no definitive studies characterizing what role CD138 plays in normal ASC development in vivo. Therefore, we compared antibody production in sdc1-deficient mice (sdc1$^{-/-}$) and wild-type (WT) control mice following immunization with NP-OVA precipitated in alum. The IgG response was significantly reduced in sdc1$^{-/-}$ mice at all measured time points with a greater than threefold reduction by day 60 following immunization (Figure 1A). On day 7 after immunization, serum levels of anti-NP IgM in mice were weak and completely extinguished by day 28 or later (Figure 1B). At these low levels, we were not able to detect significantly reduced serum levels of IgM in WT compared with sdc1$^{-/-}$ mice, but there was a slight trend similar to that of IgG.

Next, we quantified the number of NP-specific IgG ASCs in the LNs of mice using ELISPOT on day 8 following immunization. We found fewer NP-specific IgG$^+$ ASCs in the LNs of sdc1$^{-/-}$ mice compared with WT controls (Figure 1D), consistent with the ELISA data. Because CD138 is a critical surface marker for ASC identification and is not expressed in sdc1$^{-/-}$ mice, we bred sdc1$^{-/-}$ mice with Blimp1-YFP reporter allele, which expresses YFP in ASCs[22] and allows analysis of ASCs by flow cytometry. Analysis of YFP$^+$ NP-specific ASCs on day 8 after immunization showed decreased ASCs in sdc1$^{-/-}$ compared with WT mice, both in IgG$^+$ and IgM$^+$ ASC subsets (Figure 1E), confirming the ELISPOT and ELISA measurements. Numbers of IgM$^+$ ASCs were extremely low confirming our ELISA data, however, we see a similar proportion of IgG to IgM in the sdc1$^{-/-}$ mice (Figure 1E). To assess the long-term effects of sdc1 deficiency on ASCs, we examined NP-specific ASCs in the BM by ELISPOT on day 60 following immunization and found fewer cells in sdc1$^{-/-}$ mice compared with WT mice (Figure 1F). We conclude that CD138 is required for long-term humoral immunity.

Because ASCs can arise from extrafollicular responses or germinal centers (GCs), we assessed if changes in humoral responses were as a result of poor B- or T-cell responses. However, we found no difference in the frequency of TFH cells, TFR cells, and GC B cells in sdc1$^{-/-}$ mice compared with WT controls on day 7 after immunization (Figure 1G-I). In addition, affinity maturation was not altered in sdc1$^{-/-}$ mice compared with WT mice (Figure 1C). Thus, the defect in the IgG antibody response after immunization of sdc1$^{-/-}$ mice was not caused by a weaker GC reaction, consistent with the initiation of CD138 expression only at the plasmablast cell stage following GC exit.[22,23]

CD138 promotes ASC accumulation and maturation

Because sdc1$^{-/-}$ mice lack CD138 in all cell types, including endothelial cells, HSCs, and lymphocyte precursors, it is difficult to assess if the defect in ASC accumulation is cell autonomous. Therefore, we developed an antigen-specific model to track the cell intrinsic role of CD138 in CD138 sufficient hosts. To track antigen-specific ASCs in vivo, we bred WT and sdc1$^{-/-}$ mice expressing the Blimp-1-YFP$^+$ allele, which is expressed in both WT and sdc1-deficient ASCs equally well, together with the B1-8^{high} heavy chain Ig allele, which produces a high-affinity NP-specific B-cell receptor (when matched with λ light chain).[24] Purified naïve B cells from these donor mice were co-transferred into WT recipients (as in Figure 2A), which allowed us to compare responses in the same host and assess any cell-intrinsic defects
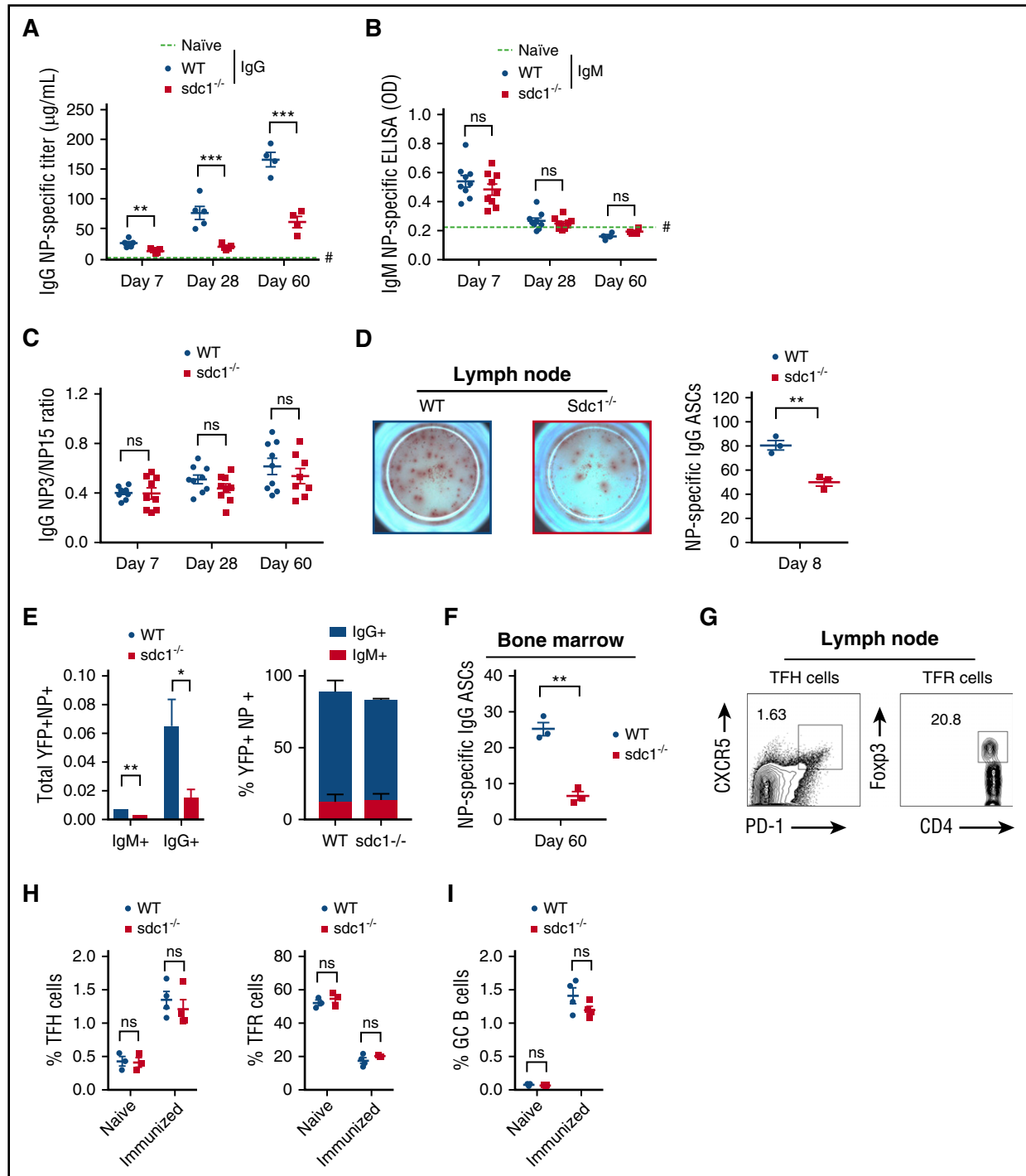
Figure 1. The post-GC humoral immune response is compromised in the absence of CD138 expression. (A-C) Mice lacking CD138 expression (sdc1$^{-/-}$) or WT mice were immunized subcutaneously with NP(16)-OVA precipitated in alum and bled on the indicated days. (A) NP-specific levels of total IgG were measured by ELISA. Quantification represents μg/mL IgG. Dotted line highlighted by # represents the mean NP-specific IgG response of unimmunized naïve mice. (B) NP-specific levels of total IgM were measured by ELISA. Quantification represents O.D. Dotted line highlighted by # represents the mean NP-specific IgM response of unimmunized naïve mice. (C) ELISA was used to examine affinity maturation by measuring the ratio from the binding of low-affinity IgG to NP(15) and higher-affinity IgG binding to NP(3). (D) A representative ELISPOT image of draining LN cells from WT or sdc1$^{-/-}$ mice 8 days after immunization. Graph shows quantification (mean ± SEM) of NP-specific IgG ASCs per 10^6 LN cells. (E) Graph depicts the total number of IgM$^+$ or IgG$^+$ antigen-specific (NP$^+$YFP$^+$) ASCs in the LN of immunized WT and sdc1$^{-/-}$ mice (left). Stacked bar graph shows the percentage of IgM$^+$ or IgG$^+$ antigen-specific (NP$^+$) YFP$^+$ ASCs on day 8 following immunization of WT and sdc1$^{-/-}$ mice (right). (F) ELISPOT analysis of BM cells from WT and sdc1$^{-/-}$ mice 60 days after immunization. Graph represents mean (± SEM) of the number of NP-specific ASCs per 10^6 BM cells. (G-H) CD4$^+$B220$^-$ PD-1$^+$CXCR5$^+$Foxp3$^-$ TFH cells and CD4$^+$B220$^-$PD-1$^+$CXCR5$^+$Foxp3$^+$ TFR cells were examined by flow cytometry on day 7 following immunization of WT or sdc1$^{-/-}$ mice. Gating strategy and representative dot plots of TFH and TFR cells are shown. (G). Graphs show the percentage of TFH or TFR cells in the LN of non-immunized (naïve) and immunized mice. (I) B220$^+$GL7$^+$Fas$^+$ GC B cells were measured by flow cytometry on day 7 following immunization. Graph represents the percentage of GC B cells in either naïve or immunized WT or sdc1$^{-/-}$ mice. *$P < .05$; **$P < .01$; ***$P < .001$. ns, not significant; O.D., optical density; TFH, T follicular helper; TFR, T follicular regulatory.
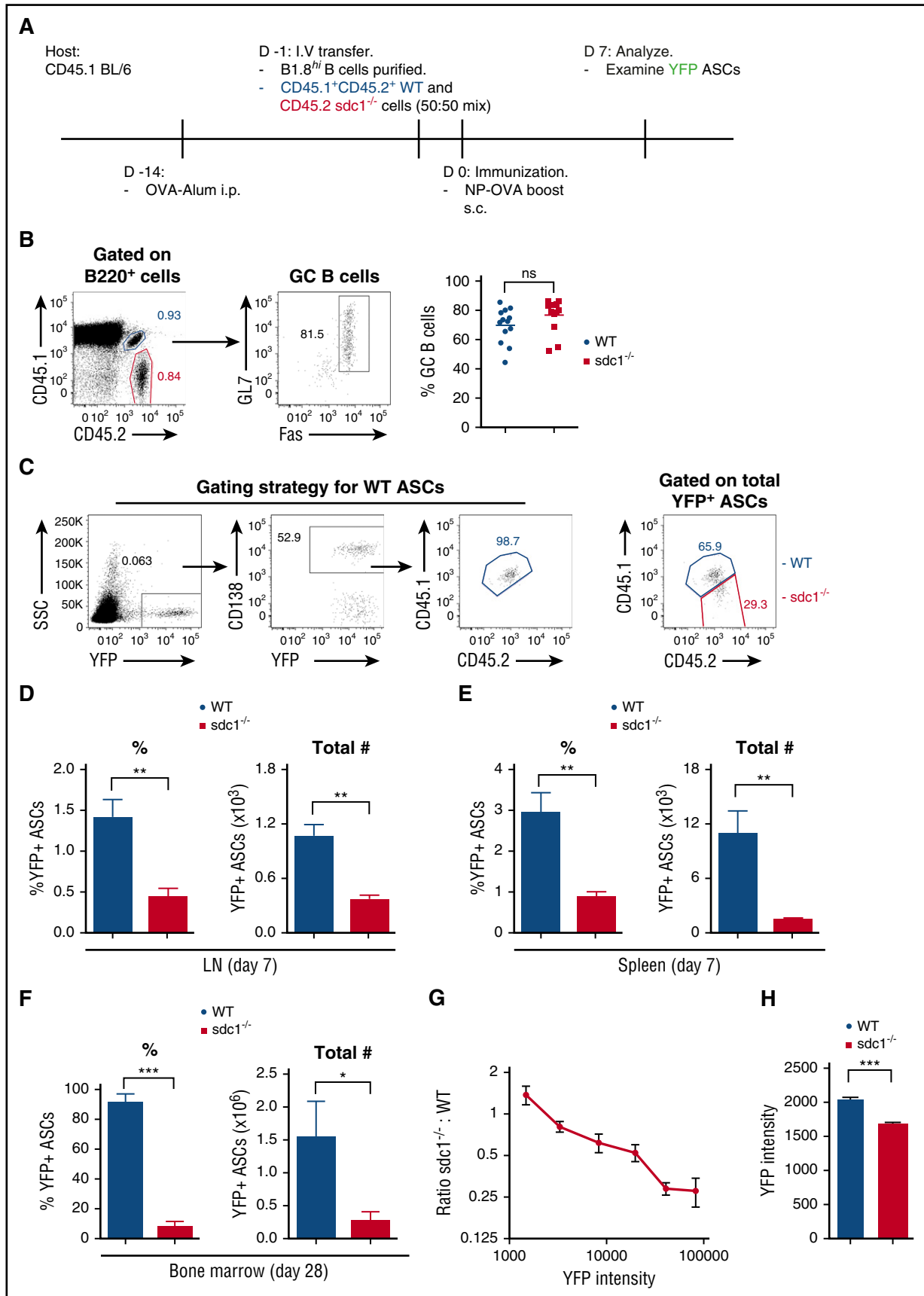
Figure 2. CD138 expression promotes ASC accumulation and maturation. (A) Diagrammatic representation of the cell transfer and immunization protocol. CD45.1/2 WT cells and CD45.2 sdc1$^{-/-}$ cells were injected at a ratio of 50:50. (B) Gating strategy and representative dot plots of B220^{+}GL7^{+}Fas^{+} GC B cells from WT (blue; co-stained for CD45.1 and CD45.2) and sdc1$^{-/-}$ (red; CD45.2^{+}) cells 7 days after secondary immunization. Graph represents the percentage of GC B cells generated on

during ASC differentiation. On day 7 post-boost with NP-OVA, we measured the peak production of NP-specific (YFP$^+$) ASCs. A stringent gating strategy combining congenic markers (CD45.1$^+$ CD45.2$^+$) and CD138 expression was used to identify WT and sdc1-deficient ASCs derived from the transferred B cells (Figure 2C). Both WT and sdc1$^{-/-}$ B cells expanded and differentiated into GC B cells (Fas$^+$GL7$^+$) to a similar extent after immunization (Figure 2B), consistent with direct immunization of WT and sdc1$^{-/-}$ mice (Figure 1I). Notably, we found that both the total numbers and frequency (normalized to subset size) of WT NP-specific YFP$^+$ ASCs in the draining LN were threefold higher than sdc1$^{-/-}$ ASCs (Figure 2C-D). To confirm these results, we used a primary immunization approach of NP-OVA emulsified in alum and examined YFP$^+$ ASC generation on day 8 obtaining similar results (data not shown). To compare if these effects were organ specific, we used IP direct immunization of NP-OVA in alum and found ASCs generated in the spleen were also derived predominantly from WT B cells (Figure 2E). Consistent with the LN and spleen data on day 7, we observed significantly more WT ASCs in the BM 28 days following primary immunization (Figure 2F).

Blimp-1 levels increase during PC differentiation, with the most fully mature cells expressing the highest levels.[25] Similarly, Blimp-1-YFP reporter expression starts at the plasmablast stage and increases with PC differentiation,[22] as does the Blimp-1–green fluorescent protein reporter.[26] We found that sdc1-deficient ASCs had lower YFP levels compared with WT ASCs both in vivo and in situ (Figure 2G-H). Within the YFP^{low} range of ASCs, we observed no difference in the numbers of WT vs sdc1$^{-/-}$ ASCs, but in the YFP^{high} gate, ASCs were predominately WT derived (Figure 2G). Therefore, the failure to detect equivalent numbers of YFP^{high} sdc1$^{-/-}$ ASCs suggests a failure during late maturation or defects in survival pathways found exclusively in fully mature ASCs.

ASCs lacking CD138 are more prone to apoptosis

We next assessed whether defects in differentiation, proliferation, or survival pathways could account for the lack of YFP^{high} sdc1$^{-/-}$ ASCs. To assess ASC differentiation, we generated in vitro B-cell blasts from mixed cultures of WT and sdc1$^{-/-}$ naïve B cells using LPS, and observed no difference in proliferation rate (Figure 3A) or plasmablast differentiation (YFP generation) on day 3 (Figure 3B-C). However, by day 6 of culture, as plasmablasts began to die, we observed a reduced percentage of YFP$^+$ cells in the sdc1$^{-/-}$ population compared with WT cells suggesting a potential survival defect (Figure 3C). Although we did not observe significant differences in apoptosis between total WT and sdc1$^{-/-}$ plasmablasts in vitro cultures (data not shown), we did find that among WT plasmablasts, apoptosis was occurring exclusively within the immature CD138$^-$ subset, both by Annexin V$^+$ and cleaved caspase 3$^+$ measurements (Figure 3D). Furthermore, we examined human ASCs from peripheral blood of healthy donors and identified CD138$^+$ and CD138$^-$ subpopulations within the CD19^{low}CD20$^-$ CD38^{high} compartment. Similar to murine ASCs, the CD138$^+$ fraction was less prone to apoptosis (Figure 3E).

Next, we assessed ASC survival and proliferation in vivo. Consistent with the in vitro data, sdc1$^{-/-}$ ASCs proliferation was similar to WT ASCs, based on Ki-67 labeling (Figure 3K). However, sdc1$^{-/-}$ ASCs were more apoptotic compared with WT ASCs, both by Annexin V (Figure 3F) and cleaved caspase 3 staining (data not shown), but we found no survival difference in the YFP-negative, non-ASC populations of transferred cells, suggesting the defect was ASC specific (Figure 3F). On day 7, within the YFP$^+$ ASC WT population, there are both CD138$^+$ and CD138$^-$ subsets reflecting mature and immature ASCs populations, respectively.[22] We found that the WT CD138$^-$ fraction was approximately sixfold more apoptotic than the CD138$^+$ fraction (Figure 3G).

To assess apoptosis in situ, we used our transfer model as before, but only transferred either WT or sdc1$^{-/-}$ donor B cells into recipient mice, and assessed apoptosis directly using time-lapse intravital two-photon imaging in the medullary cords of the popliteal LN on day 7 after immunization. Using this approach, we observed and scored an increased frequency of apoptotic events (based on membrane blebbing leading to cell rupture) in sdc1$^{-/-}$ ASCs as compared with WT ASCs (Figure 3H; supplemental Movie 1, available on the *Blood* Web site), which correlated with our ex vivo results.

Next, we assessed if changes to pro-survival factors known to be involved in ASC survival were altered in CD138-deficient ASCs. We compared WT and sdc1-deficient ASCs generated in vivo following immunization for expression of Bcl-2 and Mcl-1,[28] both implicated in PC survival. We found greater expression of the pro-survival proteins Bcl-2 and Mcl-1 in WT ASCs compared with sdc1-deficient ASCs (Figure 3I-J). Within the WT ASC population that is composed of both mature (CD138$^+$) and immature (CD138$^-$) ASCs, Bcl-2 and Mcl-1 were preferentially expressed in the CD138$^+$ fraction (Figure 3I-J). Collectively, these data show that surface expression of CD138 on ASCs does not impact early ASC differentiation or proliferation, but rather promotes or correlates with cell survival of mature CD138$^+$ ASCs.

ASCs lacking CD138 have reduced levels of IL-6 signaling

Although CD138 is largely incapable of signaling alone, it has been shown to function as a co-receptor in nonhematopoietic cells[29] and can bind cytokines via its HS chains, including APRIL, that promotes ASC survival in the BM.[30] Similarly, IL-6, an important factor in both ASC maturation and survival, has been shown to bind to HS[31] and CD138.[32] Sdc1$^{-/-}$ mice have also been reported to have higher IL-6 serum levels.[32] Therefore, we investigated if the defect in sdc1$^{-/-}$ ASC survival was related to pro-survival cytokine signaling.

To assess if IL-6 signaling in ASCs is dependent on CD138 expression, we examined levels of pSTAT3, which is a transcription factor that functions downstream of IL-6 receptor activation.[33] Using our co-transfer model system as before (Figure 2A), we measured pSTAT3 levels on ex vivo NP-specific (YFP$^+$) ASCs on day 7 following immunization. Steady-state levels of pSTAT3 in ASCs were undetectable ex vivo (data not shown). Therefore, we stimulated

---

Figure 2 (continued) day 7 following immunization. (C) Gating strategy showing the detection by flow cytometry of NP-specific YFP$^+$ ASCs on day 7 following immunization. WT (blue) ASCs co-stain for CD45.1 and CD45.2, whereas ASCs lacking CD138 expression (red) stain for CD45.2 only. CD138 expression was used to delineate WT gating. (D-E) Percentage (left) and frequency (right) of WT and CD138-deficient ASCs in the LN (D) and spleen (E) of host mice on day 7 after immunization. Results are expressed relative to total transferred B cells. Mice were immunized with NP-OVA either by a subcutaneous route in the case of LN data or by IP immunization for spleen data. (F) Percentage and frequency of WT and CD138-deficient ASCs in the BM of host mice 28 days after primary immunization with NP-KLH emulsified in alum. (G) ASC maturation is characterized by increased YFP expression. Maturation was measured by examining the mean fluorescence intensity (MFI) of YFP expression in sdc1-deficient ASCs relative to WT ASCs (sdc1$^{-/-}$:WT). (H) YFP$^+$ ASCs from WT or CD138-deficient ASCs in the medulla of surgically exposed LNs were examined by two photon microscopy on day 7 following immunization. YFP intensity of individual cells was measured and the mean was calculated. Graph represents the mean ($\pm$ SEM) of YFP intensity from 3 independent experiments. *$P < .05$; **$P < .01$; ***$P < .001$. ns, not significant; SSC, side scatter.
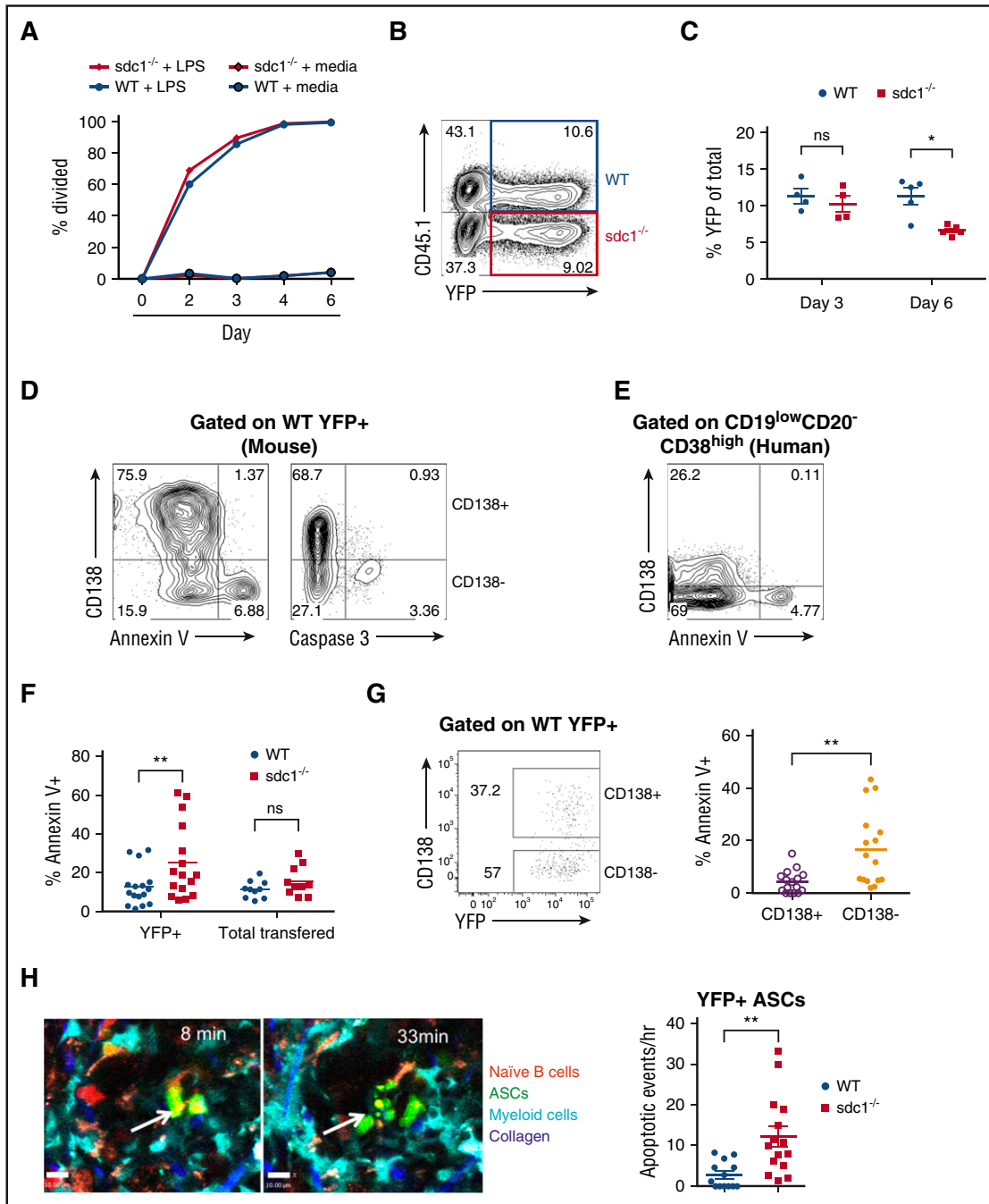
Figure 3. In vitro and in vivo ASC survival is dependent on CD138 expression. (A-D) Purified B cells from WT and sdc1-deficient mice (sdc1$^{-/-}$) were cocultured in vitro with LPS for 3 days and ASC generation (YFP$^+$) was examined. (A) Purified B cells from WT and sdc1$^{-/-}$ mice were pre-labeled with celltrace violet, and analyzed for cell division up to day 6 of culture. Resting B cells cultured in the absence of LPS were used as a control. (B) Flow cytometry gating strategy depicting a contour plot of YFP$^+$ ASCs generated following culture. WT (blue) ASCs were distinguished from CD138-deficient ASCs (red) by the expression of CD45.1 using flow cytometry. (C) The percentage of YFP$^+$ ASCs generated by in vitro culture is demonstrated on day 3 and day 6 and expressed as a percentage of total cells. (D) YFP$^+$ ASCs derived from WT B cells were examined for apoptosis on day 3 after culture with LPS. Mature CD138$^+$YFP$^+$ ASCs were distinguished from immature CD138$^-$ ASCs by flow cytometry, and apoptosis was examined using Annexin V or activated caspase 3 staining. (E) Human PBMCs were examined by flow cytometry. Gating on CD19^{low}CD20$^-$CD38^{high} cells revealed CD138$^+$ and CD138$^-$ fractions that were examined for Annexin V staining. Representative contour plots are demonstrated. (F-K) YFP$^+$ ASCs were generated in vivo following co-transfer of purified naïve B cells from WT and sdc1$^{-/-}$ mice and immunization with NP-OVA (protocol depicted in Figure 2A). (F) Cells from the dLN of immunized mice were stained for Annexin V to examine apoptosis and analyzed by flow cytometry. The percentage of apoptosis in YFP$^+$ ASCs or YFP$^-$ transferred cells is depicted (WT [blue]; sdc1$^{-/-}$ [red]). (G) Within the WT ASC compartment, mature CD138$^+$YFP$^+$ ASCs were distinguished from immature CD138$^-$ ASCs by flow cytometry. A representative dot plot is shown (left). The graph represents the percentage of cell apoptosis within the CD138$^+$ and CD138$^-$ subsets in dLN of immunized mice (right). (H) Intravital two-photon microscopy was performed on the surgically exposed popliteal LNs of immunized mice. Myeloid cells (blue), ASCs (green), naïve B cells (red), and collagen (purple) could be distinguished from one another. A representative image of an apoptotic event is depicted. Apoptotic events were recorded and quantified in a blinded manner (left). Graph represents the number of apoptotic events observed per hour (right). (I-J) Cells from the dLN of immunized mice were stained for Bcl-2 (I) or Mcl-1 (J), and analyzed by flow cytometry. Graph depicts MFI in YFP$^+$ ASCs from either WT (blue) or sdc1$^{-/-}$-derived (red) cells. Within the WT ASC compartment, mature CD138$^+$YFP$^+$ ASCs (open circles) were distinguished from immature CD138$^-$ ASCs (closed circles) by flow cytometry, and graph depicts MFI. FMO controls included. (K) dLN cells were stained with ki67 to examine proliferation by flow cytometry. WT YFP$^+$ (red) and CD138-deficient YFP$^+$ (blue) ASCs are depicted in a representative histogram. *$P < .05$; **$P < .01$; ***$P < .001$. dLN, draining lymph nodes; FMO, fluorescence minus one; ns, not significant; PBMCs, peripheral blood mononuclear cells.

Figure 3. (Continued).
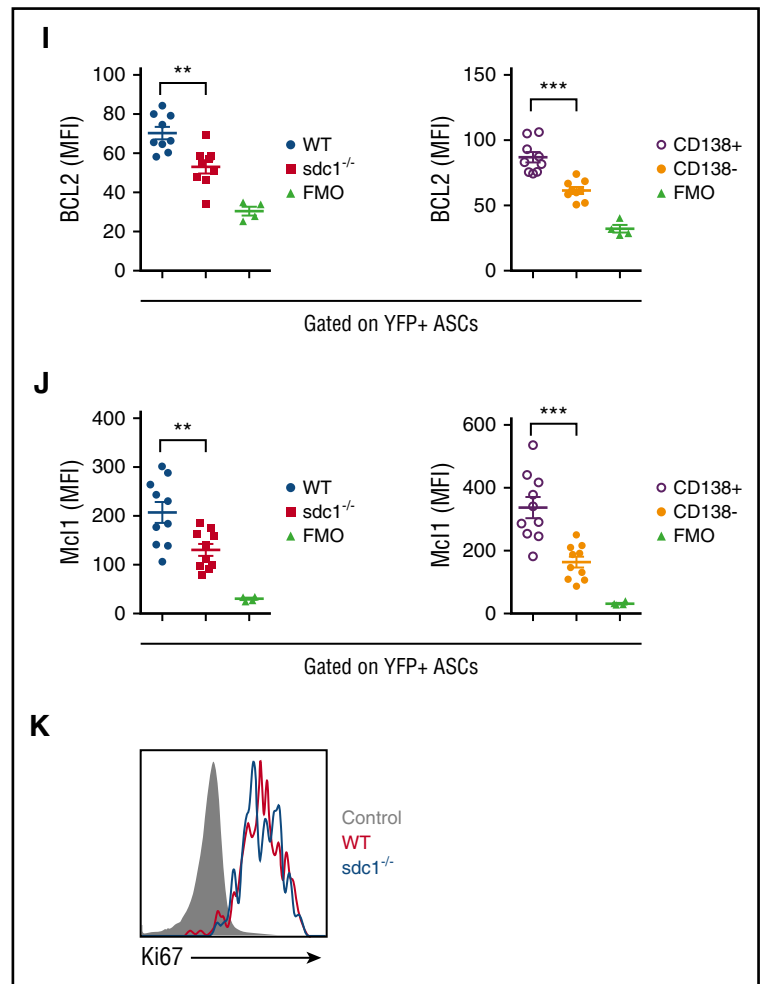
cells ex vivo with rIL-6 and found that sdc1$^{-/-}$ ASCs produced less pSTAT3 than WT ASCs (Figure 4A). Interestingly, within the YFP$^+$ WT population, ~80% of the CD138$^+$ fraction were pSTAT3$^+$ compared with ~40% of the CD138$^-$ fraction (Figure 4B), indicating that CD138 was promoting IL-6 signaling. A similar STAT3 phosphorylation pattern was observed in peripheral human CD19^{low}CD20$^-$CD38^{high} ASCs with the CD138$^+$ fraction being preferentially phosphorylated (Figure 4C).

IL-6 signaling was dependent on the IL-6 receptor because in vitro blockade of CD126 or gp130 (CD130) subunits[34] ablated phosphorylation of STAT3, equally in both WT and sdc1$^{-/-}$ ASCs (not shown). Furthermore, surface expression of CD126 and CD130 were comparable in WT and sdc1$^{-/-}$ ASCs generated in vivo (Figure 4D), ruling out changes in expression as a possible mechanism for altered pSTAT3.

To rule out any global changes in the STAT3 pathway that could correlate with ASC maturation, we tested IL-21 signaling in ASCs. IL-21 is known to activate the STAT3 pathway in B cells,[35] but unlike IL-6, it is not thought to bind to HS.[12] IL-4 and IL-13 have also recently been shown not to bind to CD138.[36] Therefore, we treated ASCs ex vivo with recombinant IL-21 and found that pSTAT3 expression was independent of CD138 expression (Figure 4E).

Based on these results and previous reports, we tested if CD138 functions by binding cytokines or enhancing receptor sensitivity. Using in vitro generated plasmablasts to measure pSTAT3 activation following IL-6 administration, we found that CD138 enhanced

efficiency of IL-6 signaling, but only at subsaturating cytokine levels (Figure 4F). Although HS is expressed on various surface proteins, we tested if CD138 expression altered total HS levels on mature ASCs, thereby promoting preferential binding of pro-survival cytokines compared with immature ASCs lacking CD138 expression. We quantified HS chains on both WT and sdc1-deficient YFP$^+$ ASCs generated in vivo and observed that total HS chains on sdc1-deficient ASCs were more than twofold decreased compared with WT CD138$^+$ ASCs (Figure 4G). Indeed, HS chain levels were comparable between the CD138-negative fraction of WT ASCs and sdc1-deficient ASCs, further supporting our contention that CD138 represents the dominant source of HS sidechains on mature ASCs. Treatment of cells with heparinase III that enzymatically removes the HS chains ablated anti-HS staining (Figure 4G). Thus, the reduction in IL-6–mediated STAT3 phosphorylation in sdc1-deficient ASCs compared with WT ASCs, as well as in the CD138$^+$ fraction of WT ASCs compared with the CD138$^-$ fraction is consistent with a reduced expression of HS sidechains in ASCs lacking CD138.

IL-6 and APRIL promote ASC survival and accumulation in a CD138-dependent manner

To test if CD138 was required for IL-6 signaling in vivo, we compared WT and sdc1$^{-/-}$ ASCs generated as before (Figure 2A) in IL-6–deficient vs WT recipients. Indeed, in IL-6$^{-/-}$ recipients, the production of YFP$^+$ ASCs was similar between WT and sdc1$^{-/-}$
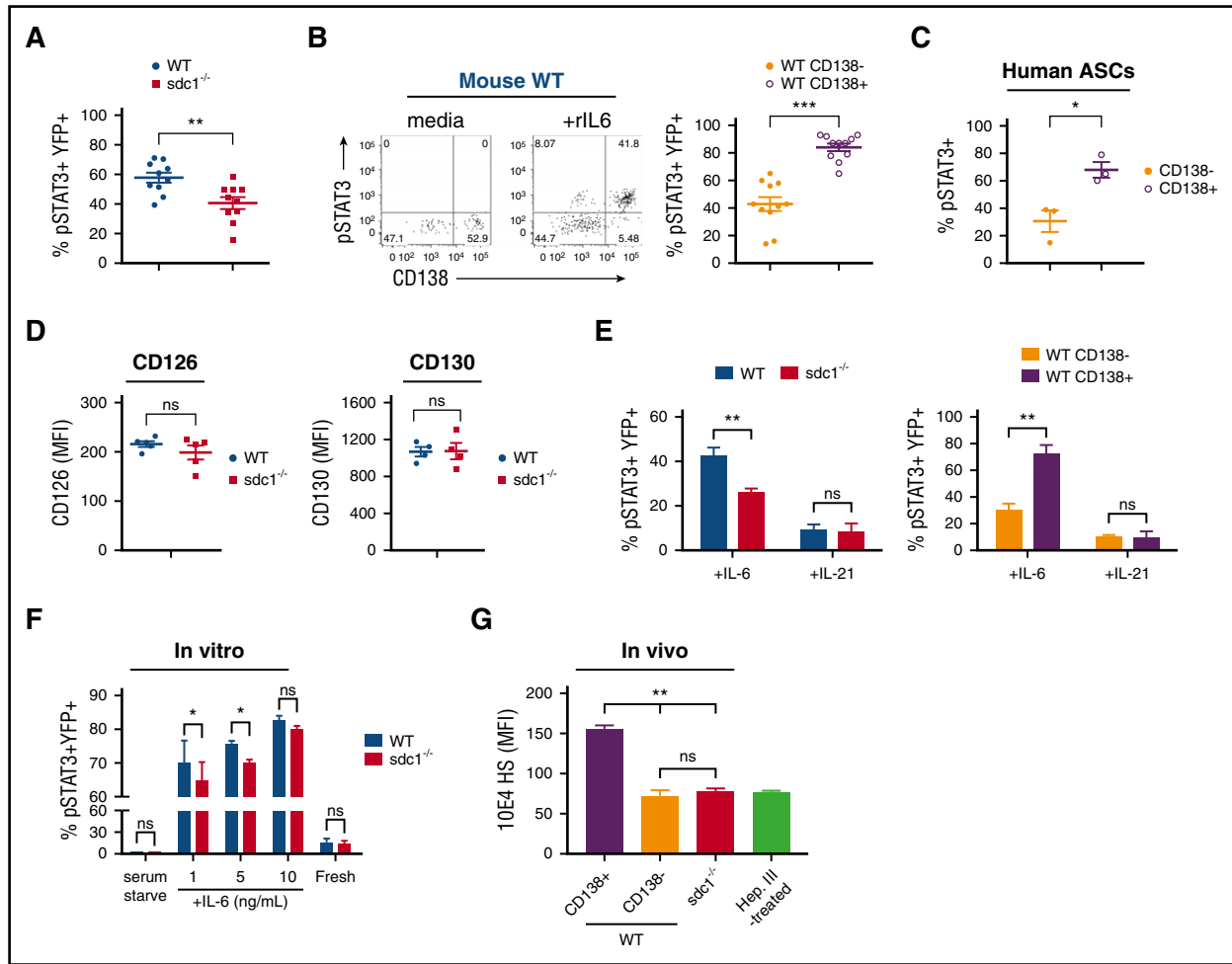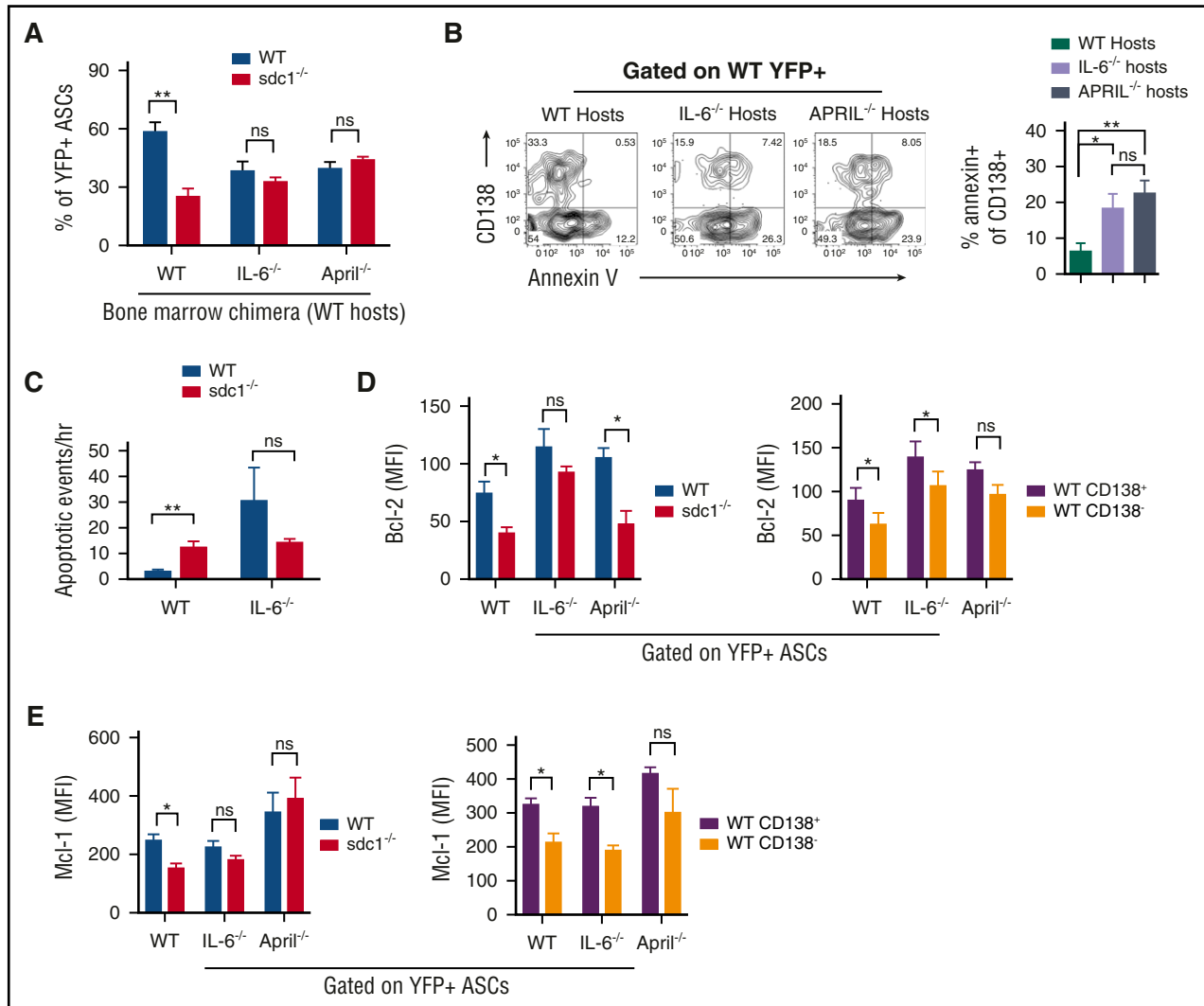
Figure 4. CD138 expression on ASCs promotes IL-6 signaling. (A-B,D) Mice were co-injected with purified transgenic B cells from WT and sdc1$^{-/-}$ mice, immunized, and examined for YFP$^+$ ASCs on day 7. (A) dLN cells were briefly serum starved, incubated in the presence of recombinant IL-6 (rIL-6) for 20 minutes and analyzed for intracellular pSTAT3 by flow cytometry. Graph represents mean ($\pm$ SEM) of YFP$^+$pSTAT3$^+$ cells. (B) Within the WT ASC compartment, mature CD138$^+$YFP$^+$ ASCs were distinguished from immature CD138$^-$YFP$^+$ ASCs by flow cytometry, and stained for pSTAT3 following ex vivo stimulation by rIL-6. Representative flow cytometry dot plots depict prior to (media) and after (+rIL6) rIL-6 stimulation (left). Graph represents mean ($\pm$ SEM) of the percentage of YFP$^+$pSTAT3$^+$ cells from each subset (right). (C) Human PBMCs were examined by flow cytometry. Graph represents mean ($\pm$ SEM) of the percentage of CD19^{low}CD38^{high} ASCs positive for pSTAT3 from within the CD138$^+$ or CD138$^-$ subsets following ex vivo stimulation by human rIL-6. (D) The dLN from immunized host mice were examined by flow cytometry. YFP$^+$ ASCs derived from either WT or sdc1-deficient B cells were examined for IL-6α receptor (CD126; left) or IL-6β (CD130; right) receptor expression. Graphs show mean of MFI from either WT (blue) or sdc1$^{-/-}$ (red) cells. (E) dLN cells from immunized mice were briefly serum starved, incubated in the presence of rIL-6 or rIL-21 (10 ng/mL) for 20 minutes, and analyzed for intracellular pSTAT3 by flow cytometry. Graphs show mean ($\pm$ SEM) of the percentage of YFP$^+$ cells stained for pSTAT3. (F) Purified B cells from WT and CD138-deficient mice (sdc1$^{-/-}$) were cocultured with LPS to generate ASCs in vitro. On day 3, cells were incubated in media in the presence (fresh) or absence (serum starved) of fetal calf serum, and stimulated with rIL-6 (either 1, 5, or 10 ng/mL). pSTAT3 levels were examined by flow cytometry. Graph depicts mean ($\pm$ SEM) of the percentage of YFP$^+$pSTAT3$^+$ cells. (G) In vivo generated YFP$^+$ ASCs were stained with 10E4 antibody to detect HS. Heparinase III-treated cells that lack HS surface expression is used as a control. Graph represents the MFI of 10E4 expression on various subsets relative to heparinase III-treated cells. *$P < .05$; **$P < .01$; ***$P < .001$. ns, not significant; PBMCs, peripheral blood mononuclear cells.

populations, in contrast to WT recipients (Figure 5A). This was due to increased apoptosis of CD138$^+$ WT ASCs in IL-6–deficient recipients not seen in WT recipients (Figure 5B). Similar results were obtained in APRIL-deficient hosts (Figure 5A-B), suggesting that both HS-binding cytokines contribute to ASC survival in the LN. Intravital imaging revealed significant increases in ASC apoptosis in IL-6 hosts, which were occurring at similar frequencies in WT and sdc1$^{-/-}$ subsets (Figure 5C; supplemental Movie 2).

Many populations of cells can produce IL-6 and APRIL in the LN,[37] however, it is unclear which population is functionally required to promote ASC survival. To assess if host-derived cytokines supporting ASC survival were produced by stromal or hematopoietic lineages, we lethally irradiated WT hosts and reconstituted with WT, IL-6$^{-/-}$ or APRIL$^{-/-}$ BM. We found that although WT BM could promote

CD138$^+$ ASC survival, both IL-6$^{-/-}$ and APRIL$^{-/-}$ BM could not, suggesting these pro-survival cytokines were produced by radiation-sensitive cells in the LN (Figure 5A). Further dissection of IL-6–secreting populations did not conclusively reveal a specific lineage of hematopoietic cells promoting ASC survival (data not shown).

To test if APRIL and IL-6 deficiencies altered pro-survival pathways in a CD138-dependent manner, we examined Bcl-2 and Mcl-1 levels in ASCs using our co-transfer model. We found that although WT ASCs, which had higher levels of Bcl-2 and Mcl-1 levels as compared with sdc1$^{-/-}$ ASCs in WT hosts (Figure 3H-I), we saw this difference diminished in IL-6 and APRIL-deficient hosts (Figure 5D-E). Similarly, we found that in the WT ASC population, CD138$^+$ ASCs has higher Bcl-2 and Mcl-1 expression than CD138$^-$ ASCs in WT hosts, but these effects were diminished

Figure 5. IL-6 and APRIL in concert with CD138 expression promote ASC survival. (A-E) Purified transgenic B cells from WT and sdc1$^{-/-}$ mice were injected into host mice in which the hematopoietic cells were either WT, IL-6 deficient (IL-6$^{-/-}$), or APRIL deficient (APRIL$^{-/-}$), and immunized and examined for YFP^{+} ASCs on day 7. (A) Graph depicts the percentage of WT and sdc1$^{-/-}$ ASCs from the LN in the different host mice. (B) WT ASCs were examined for apoptosis by Annexin V staining. Representative contour plots are shown (left). Graph depicts percentage of apoptosis in the CD138^{+} compartment of WT ASCs in WT, IL-6$^{-/-}$, or APRIL$^{-/-}$ hosts. (C) As in Figure 3H, intravital two-photon microscopy was performed on the surgically exposed popliteal LNs of immunized mice. Apoptotic events were recorded and quantified in a blinded manner. Graph represents the number of apoptotic events observed per hour. (D-E) WT and sdc1$^{-/-}$ ASCs from the LN in the different host mice were examined for intracellular expression of Bcl-2 (D) and Mcl-1 (E). Graphs depict the MFI. *$P <$ .05; **$P <$ .01. ns, not significant.

in cytokine-deficient recipients (Figure 5D-E). However, as expected, the absence of a single cytokine did not completely ablate CD138's pro-survival effect, suggesting that CD138 has pleiotropic effects, including binding multiple survival cytokines.

Collectively, these data suggest that CD138 plays a major role in the protection of mature ASCs from pre-mature apoptosis by using its HS chains to substantially increase IL-6 and APRIL presentation to their receptors on PCs, leading to increased cytokine signaling.

Discussion

Survival of ASCs is paramount for producing antibody in the acute phase of infection and ensuring sufficient time to reach long-term survival niches in BM[38] and spleen.[39] CD138 expression on ASCs has been a hallmark for identifying mature PCs; but until now, its function has been unclear. We show that although CD138 is not required to generate ASCs, its surface expression gives a survival advantage by increasing IL-6 and APRIL signaling. Even with equivalent levels of IL-6 receptor, signaling was enhanced by CD138 expression. IL-6 has long been known to be a key survival factor in PC survival,[40,41] and we demonstrate here that CD138 is central to the mechanism by which IL-6 and APRIL is able to exert its survival-promoting function. Although CD138 can be shed from mature ASCs[42] by several mechanisms including apoptosis, we find the majority of the CD138^{-} cells that were Annexin V^{+} expressed low YFP levels (data not shown), suggesting immature ASCs are the apoptotic population rather than mature ASCs that have lost CD138 surface expression. Moreover, in IL-6–deficient recipients, we find CD138 downregulation is not required for apoptosis (Figure 5B).

A prior study found that heparin, which is structurally analogous to the HS moieties on CD138, bound IL-6 and caused a fourfold decrease in the rate of IL-6 degradation.[31] Thus, we propose that CD138 expression gives more mature ASCs a survival advantage over less mature ASCs, by binding, preserving, and presenting cytokines to ASC

surface receptors,[43] in a competitive niche. This pathway would preferentially promote survival of the more mature ASCs, which express the highest levels of CD138. This may be a competitive process, ensuring survival of long-lived high affinity PCs is not compromised by the influx of newly minted plasmablasts, which could destabilize long-term immunity. Moreover, limiting immature PCs can be an important immune checkpoint, preventing excessive inflammation or the emergence of autoreactive plasmablasts, which are often immature and associated with lymphoid tissues.[44] This would explain why we and others find no overt difference in the steady-state number of ASCs in older WT vs sdc1$^{-/-}$ mice[32] (data not shown). However, in the absence of CD138, humoral responses were compromised.

CD138 is the dominant HS bearing proteoglycan on ASCs. In the absence of CD138, HS levels on ASCs were minimal. We propose CD138 may associate with the IL-6 receptor or, alternatively regulate IL-6 receptor clustering, in addition to binding the ligand IL-6. A similar model for HS has been reported for fibroblast growth factor receptor binding to its ligand.[45] In a recent study, Beauvais et al demonstrated that CD138 can complex with insulin-like growth factor-1 receptor (IGF-1R) and αVβ5 integrin, promoting autophosphorylation of IGF-1R and prevention of apoptosis in myeloma cell lines.[46] Although sdc1$^{-/-}$ ASCs had lower IGF-1R phosphorylation than WT ASCs (data not shown), we do not expect this pathway to be related to cytokine signaling, as we have shown here.

As in normal ASCs, CD138 also mediates inappropriate survival of malignant ASCs or myeloma cells. CD138 small interfering RNA knockdown promoted myeloma cell apoptosis,[47] leading to reduced growth in vivo.[48] Growth factors such as hepatocyte growth factor and epidermal growth factor also use surface bound CD138 as a co-receptor to promote malignant cell survival and proliferation in the BM.[16,17] Overall, these findings are consistent with the role of CD138 as a versatile co-receptor and suggest that CD138 might accommodate the

surface accumulation of different survival signals depending on the survival niche. Therapies directed against CD138 and IL-6/IL-6R are in various stages of clinical trial[19,49,50] and based on our results, should have implications on long-term immune function.

Acknowledgments

Authorship

Contribution: M.J.M. designed and performed experiments, analyzed the data, and wrote the manuscript; P.W.P. provided the sdc1 knockout mice and advice; and D.R.F. designed and performed experiments, analyzed the data, wrote the manuscript, and supervised the study.

Conflict-of-interest disclosure: The authors declare no competing financial interests.

Correspondence: David R. Fooksman, Albert Einstein College of Medicine, 1300 Morris Park Ave, Bronx, NY 10461; e-mail: david.fooksman@einstein.yu.edu.

References

1. Nutt SL, Hodgkin PD, Tarlinton DM, Corcoran LM. The generation of antibody-secreting plasma cells. *Nat Rev Immunol.* 2015;15(3):160-171.

2. Sanderson RD, Lalor P, Bernfield M. B lymphocytes express and lose syndecan at specific stages of differentiation. *Cell Regul.* 1989;1(1):27-35.

3. Bernfield M, Götte M, Park PW, et al. Functions of cell surface heparan sulfate proteoglycans. *Annu Rev Biochem.* 1999;68:729-777.

4. Teng YH, Aquino RS, Park PW. Molecular functions of syndecan-1 in disease. *Matrix Biol.* 2012;31(1):3-16.

5. Saunders S, Jalkanen M, O'Farrell S, Bernfield M. Molecular cloning of syndecan, an integral membrane proteoglycan. *J Cell Biol.* 1989;108(4):1547-1556.

6. Stepp MA, Gibson HE, Gala PH, et al. Defects in keratinocyte activation during wound healing in the syndecan-1-deficient mouse. *J Cell Sci.* 2002;115(pt 23):4517-4531.

7. Koda JE, Rapraeger A, Bernfield M. Heparan sulfate proteoglycans from mouse mammary epithelial cells. Cell surface proteoglycan as a receptor for interstitial collagens. *J Biol Chem.* 1985;260(13):8157-8162.

8. Freissler E, Meyer auf der Heyde A, David G, Meyer TF, Dehio C. Syndecan-1 and syndecan-4 can mediate the invasion of OpaHSPG-expressing Neisseria gonorrhoeae into epithelial cells. *Cell Microbiol.* 2000;2(1):69-82.

9. Stewart MD, Ramani VC, Sanderson RD. Shed syndecan-1 translocates to the nucleus of cells delivering growth factors and inhibiting histone

acetylation: a novel mechanism of tumor-host cross-talk. *J Biol Chem.* 2015;290(2):941-949.

10. Beauvais DM, Ell BJ, McWhorter AR, Rapraeger AC. Syndecan-1 regulates alphavbeta3 and alphavbeta5 integrin activation during angiogenesis and is blocked by synstatin, a novel peptide inhibitor. *J Exp Med.* 2009;206(3):691-705.

11. Rapraeger AC. Syndecan-regulated receptor signaling. *J Cell Biol.* 2000;149(5):995-998.

12. Coombe DR. Biological implications of glycosaminoglycan interactions with haemopoietic cytokines. *Immunol Cell Biol.* 2008;86(7):598-607.

13. Casu B, Naggi A, Torri G. Heparin-derived heparan sulfate mimics to modulate heparan sulfate-protein interaction in inflammation and cancer. *Matrix Biol.* 2010;29(6):442-452.

14. Hayashida K, Bartlett AH, Chen Y, Park PW. Molecular and cellular mechanisms of ectodomain shedding. *Anat Rec (Hoboken).* 2010;293(6):925-937.

15. Moreaux J, Sprynski AC, Dillon SR, et al. APRIL and TACI interact with syndecan-1 on the surface of multiple myeloma cells to form an essential survival loop. *Eur J Haematol.* 2009;83(2):119-129.

16. Derksen PW, de Gorter DJ, Meijer HP, et al. The hepatocyte growth factor/Met pathway controls proliferation and apoptosis in multiple myeloma. *Leukemia.* 2003;17(4):764-774.

17. Mahtouk K, Cremer FW, Rème T, et al. Heparan sulphate proteoglycans are essential for the myeloma cell growth activity of EGF-family

ligands in multiple myeloma. *Oncogene.* 2006;25(54):7180-7191.

18. Seidel C, Sundan A, Hjorth M, et al. Serum syndecan-1: a new independent prognostic marker in multiple myeloma. *Blood.* 2000;95(2):388-392.

19. Reijmers RM, Spaargaren M, Pals ST. Heparan sulfate proteoglycans in the control of B cell development and the pathogenesis of multiple myeloma. *FEBS J.* 2013;280(10):2180-2193.

20. Alexander CM, Reichsman F, Hinkes MT, et al. Syndecan-1 is required for Wnt-1-induced mammary tumorigenesis in mice. *Nat Genet.* 2000;25(3):329-332.

21. Shih TA, Roederer M, Nussenzweig MC. Role of antigen receptor affinity in T cell-independent antibody responses in vivo. *Nat Immunol.* 2002;3(4):399-406.

22. Fooksman DR, Schwickert TA, Victora GD, Dustin ML, Nussenzweig MC, Skokos D. Development and migration of plasma cells in the mouse lymph node. *Immunity.* 2010;33(1):118-127.

23. Jego G, Bataille R, Pellat-Deceunynck C. Interleukin-6 is a growth factor for nonmalignant human plasmablasts. *Blood.* 2001;97(6):1817-1822.

24. Shih TA, Meffre E, Roederer M, Nussenzweig MC. Role of BCR affinity in T cell dependent antibody responses in vivo. *Nat Immunol.* 2002;3(6):570-575.

25. Angelin-Duclos C, Cattoretti G, Lin KI, Calame K. Commitment of B lymphocytes to a plasma cell fate is associated with Blimp-1 expression in vivo. *J Immunol.* 2000;165(10):5462-5471.

26. Kallies A, Hasbold J, Tarlinton DM, et al. Plasma cell ontogeny defined by quantitative changes in blimp-1 expression. *J Exp Med.* 2004;200(8): 967-977.

27. Mérino D, Khaw SL, Glaser SP, et al. Bcl-2, Bcl-x(L), and Bcl-w are not equivalent targets of ABT-737 and navitoclax (ABT-263) in lymphoid and leukemic cells. *Blood.* 2012;119(24):5807-5816.

28. Peperzak V, Vikström I, Walker J, et al. Mcl-1 is essential for the survival of plasma cells. *Nat Immunol.* 2013;14(3):290-297.

29. Parish CR. The role of heparan sulphate in inflammation. *Nat Rev Immunol.* 2006;6(9): 633-643.

30. O'Connor BP, Raman VS, Erickson LD, et al. BCMA is essential for the survival of long-lived bone marrow plasma cells. *J Exp Med.* 2004; 199(1):91-98.

31. Mummery RS, Rider CC. Characterization of the heparin-binding properties of IL-6. *J Immunol.* 2000;165(10):5671-5679.

32. Zhang X, Wu C, Song J, Götte M, Sorokin L. Syndecan-1, a cell surface proteoglycan, negatively regulates initial leukocyte recruitment to the brain across the choroid plexus in murine experimental autoimmune encephalomyelitis. *J Immunol.* 2013;191(9):4551-4561.

33. Heinrich PC, Behrmann I, Haan S, Hermanns HM, Müller-Newen G, Schaper F. Principles of interleukin (IL)-6-type cytokine signalling and its regulation. *Biochem J.* 2003;374(pt 1):1-20.

34. Hunter CA, Jones SA. IL-6 as a keystone cytokine in health and disease. *Nat Immunol.* 2015;16(5): 448-457.

35. Berglund LJ, Avery DT, Ma CS, et al. IL-21 signalling via STAT3 primes human naive B cells to respond to IL-2 to enhance their differentiation into plasmablasts. *Blood.* 2013;122(24): 3940-3950.

36. Xu J, Park PW, Kheradmand F, Corry DB. Endogenous attenuation of allergic lung inflammation by syndecan-1. *J Immunol.* 2005; 174(9):5758-5765.

37. Mohr E, Serre K, Manz RA, et al. Dendritic cells and monocyte/macrophages that create the IL-6/APRIL-rich lymph node microenvironments where plasmablasts mature. *J Immunol.* 2009;182(4): 2113-2123.

38. Chu VT, Berek C. The establishment of the plasma cell survival niche in the bone marrow. *Immunol Rev.* 2013;251(1):177-188.

39. Smith KG, Hewitson TD, Nossal GJ, Tarlinton DM. The phenotype and fate of the antibody-forming cells of the splenic foci. *Eur J Immunol.* 1996;26(2):444-448.

40. Kopf M, Le Gros G, Coyle AJ, Kosco-Vilbois M, Brombacher F. Immune responses of IL-4, IL-5, IL-6 deficient mice. *Immunol Rev.* 1995;148: 45-69.

41. Chu VT, Beller A, Nguyen TT, Steinhauser G, Berek C. The long-term survival of plasma cells. *Scand J Immunol.* 2011;73(6):508-511.

42. Ramani VC, Pruett PS, Thompson CA, DeLucas LD, Sanderson RD. Heparan sulfate chains of syndecan-1 regulate ectodomain shedding. *J Biol Chem.* 2012;287(13):9952-9961.

43. Park PW, Reizes O, Bernfield M. Cell surface heparan sulfate proteoglycans: selective regulators of ligand-receptor encounters. *J Biol Chem.* 2000;275(39):29923-29926.

44. William J, Euler C, Shlomchik MJ. Short-lived plasmablasts dominate the early spontaneous rheumatoid factor response: differentiation pathways, hypermutating cell types, and affinity maturation outside the germinal center. *J Immunol.* 2005;174(11):6879-6887.

45. Allen BL, Filla MS, Rapraeger AC. Role of heparan sulfate as a tissue-specific regulator of FGF-4 and FGF receptor recognition. *J Cell Biol.* 2001;155(5):845-858.

46. Beauvais DM, Jung O, Yang Y, Sanderson RD, Rapraeger AC. Syndecan-1 (CD138) suppresses apoptosis in multiple myeloma by activating IGF1 receptor: prevention by synstatin IGF1R inhibits tumor growth. *Cancer Res.* 2016;76(17): 4981-4993.

47. Wu YH, Yang CY, Chien WL, Lin KI, Lai MZ. Removal of syndecan-1 promotes TRAIL-induced apoptosis in myeloma cells. *J Immunol.* 2012; 188(6):2914-2921.

48. Yang Y, MacLeod V, Dai Y, et al. The syndecan-1 heparan sulfate proteoglycan is a viable target for myeloma therapy. *Blood.* 2007;110(6):2041-2048.

49. Barbouri D, Afratis N, Gialeli C, Vynios DH, Theocharis AD, Karamanos NK. Syndecans as modulators and potential pharmacological targets in cancer progression. *Front Oncol.* 2014;4:4.

50. Tai YT, Anderson KC. Antibody-based therapies in multiple myeloma. *Bone Marrow Res.* 2011; 2011:924058.